

Full Length Research Paper

Numerical and laboratory investigation of effect of soil reinforcement on settlement of strip foundations

Forough Ashkan^{1*} and Hossein Sadighi²

¹Faculty Member, Department of Civil Engineering, University of Maragheh, Iran, Iran.

²Isfahan University of Technology, Department of Civil Engineering, Isfahan, Iran

Received 4 July, 2020; Accepted 26 August, 2020

Reinforcement of loose soils with geosynthetics in order to achieve a strengthened soil-reinforcement system, with enhanced tensile strength and reduced settlement is an important subject in the field of geotechnical engineering. In this study, a soil reinforcement system was used to increase the bearing capacity of sandy soil beneath a strip foundation. A small-scale laboratory model was built to investigate the behavior of geosynthetic reinforced sandy soil. The displacement vectors of the soil and bearing capacity of the strip foundation, in reinforced and non-reinforced states were measured to investigate the impact of several parameters, including the type of reinforcement, number of the reinforcement layers, depth of first layer of the reinforcement, and width of the reinforcement. Compared to non-reinforced and geotextile-reinforced models, the geogrid-reinforced model generally had large mass of reinforced soil with higher resistance to loading, which resulted in higher bearing capacity. Similar impacts were observed after increasing the number and width of reinforcement layers. Evaluation of the performance of reinforcements and sandy soil in the physical model with the PIV method and in the numerical simulation showed an increase in the volume of fault wedge and consequently an increase in the bearing capacity of the strip foundation.

Key words: Strip foundation, reinforced sandy soil, laboratory model (PIV).

INTRODUCTION

Geosynthetic reinforcement is a modern method of improving soil conditions and stabilizing soil slopes (Kothari and Momayez, 2018). In recent years, the behavior of geosynthetic reinforced clayey and sandy soils have been the subject of many studies (Oyawale and Ocan, 2020; Alaminikuma and Omigie, 2020; Wu et al., 2020).

With the increasing expansion of many cities in many parts of the world, the construction of buildings and roads

near mountain slopes have become a growing geotechnical engineering problem. This problem is more prevalent in urban areas situated in mountainous terrains, where there is no sufficient space to construct buildings, roads, bridges, etc. and therefore, the foundations of these structures must be inevitably placed on soil and rock slopes (Daoud et al., 2020). In such cases, poor assessment of the load-bearing capacity of the foundation and stability of the slopes can do irreparable

*Corresponding author. E-mail: ashkan@maragheh.ac.ir.

damage to the building and endanger its inhabitants.

One of the most important elements of stability analysis of soil structures is the failure mechanism. Although the failure mechanisms of many of these structures, including slopes, are well understood, the presence of reinforcements can alter their behavior and make it difficult to determine which mechanism to use in the analyses. There is ample evidence showing that geosynthetics can significantly improve the load-bearing capacity of foundations. Early experiments carried out by Biquet and Lee (1975) showed that geosynthetics can decrease the settlement of strip foundations.

In laboratory experiments of Guido et al. (1986), on square foundation resting on geotextile-reinforced sandstone, the best load-bearing capacity was observed in the model with three geotextile layers and U/B ratio of 0.5 (where U is the depth of the first reinforcement layer and B is the width of the foundation).

In a study by Bergado et al. (2002) on a geotextile-reinforced embankment, situated on soft soil, the behavior of the system throughout construction and until failure was analyzed with Plaxis software, with the results showing that geotextile can reduce plastic deformation of embankment. Chang and Cassante (2006) conducted a laboratory study, combined with numerical analysis on a square foundation, resting on geocentric-reinforced sand, and examined the effect of reinforcement on the stiffness and load-bearing capacity.

Huang and Menq, (1997) used a static analysis method, based on the limit equilibrium method to study the behavior of a horizontally reinforced sandy soil, the effects of the arrangement and properties of the reinforcements, and the failure pattern of the reinforced sand. The study reported high degree of consistency between outputs of the proposed model and the measurements obtained from the laboratory model.

Yamamoto et al. (1998) investigated the progressive failure behavior of a reinforced foundation by preparing series of laboratory loading tests, which involved simulating the ground by aluminum rods, where reinforcements had different lengths and properties. Through these tests, an image processing analysis was performed to determine the bearing capacity and mechanism of progressive failure in the test specimens. The results of the study showed that the deformation properties of the reinforced foundation were different from those of the non-reinforced, and depend on the strength, number of layers, width, depth and flexural stiffness of the reinforcing material. Under the test conditions, the effects were found to be more strongly influenced by the width and number of layers than the flexural strength of the reinforcement.

Satvati et al. (2020, 2016a, b) investigated the effects of different geosynthetics with planar and cylindrical shapes on bearing capacity of the shallow footings adjacent to a soil slope. Their results showed that

cylindrical geosynthetics (braid elements) resulted in higher bearing capacity compared to planar geogrids. These findings were reported due to the enclosure that cylindrical geosynthetics provided. In addition, effects of the other design factors, including footing width, depth of the first layer of reinforcement, number of reinforced layers, and the horizontal distance of the footing to the edge of the slope were investigated.

Chen and Abu-Farsakh (2015) provided a series of analytical solutions for estimating the ultimate bearing capacity of reinforced strip foundations. They proposed a general failure mechanism and used it to perform a limit equilibrium stability analysis for these foundations. The study showed that the depth of the punching shear failure zone (DP) depends on the relative strength of the reinforced soil layer and the underlying unreinforced soil layer and is directly related to the reinforced ratio (Rr).

As the above review shows, enhancement of the bearing capacity of reinforced soils has been the subject of many studies. In this study, the bearing capacity of reinforced and non-reinforced soils was investigated by physical modeling, using the PIV method and numerical simulation with PLaxis. Also, the soil displacement vectors in the models were compared in order to compare the soil failure mechanism with that of Das 2017.

MATERIALS AND METHODS

Specifications of the laboratory model

In this study, the models were made with dry sand of Sufian region of East Azarbaijan province in northwestern Iran. To obtain reliable results, the physical models had to be made with the sand at loose state, with relative density of 15 to 50%. To determine the characteristics of the sand, grading tests were performed according to ASTM D 422-87. The test results showed that the sand had an angle of internal friction $\phi=27^\circ$, cohesion $c = 32 \text{ kN/m}^2$ specific gravity of $G_s=2.67$, and unit weight of 1.5 g/cm^3 at loose state. The sand had uniformity coefficient $C_u=1.25$, coefficient of curvature $C_c=0.996$ and was classified as poorly graded sand (SP). The grading curve of the sand is shown in Figure 1. The elastic modulus (E) of the soil was measured by triaxial testing, which is the best method to determine this parameter.

The reinforced soil foundation base models were formed with two types of reinforcement: geogrid and geotextile. First, a reinforced concrete strip foundation with a length of 1.8 m, a width of 0.40 m, and a height of 0.50 m was created. Base plates were installed at the two ends of this foundation with 6 bolts in a way that columns could be easily attached and detached and the test system could be relocated when needed. The beam and column connections were designed in the same way. As shown in Figure 2, the columns were made by welding two UNP-160 profiles, and the beams were made by welding two UNP-200 profiles together. The created beams and columns were reinforced with band and gusset plates. The frame structure built for the loading system is shown in Figure 2.

The container in which the soil was placed was made with 3.9 mm thick metal plates of size $1.00 \times 0.30 \times 0.60 \text{ m}$, which were acceptably rigid for their size and the type of connections. A series

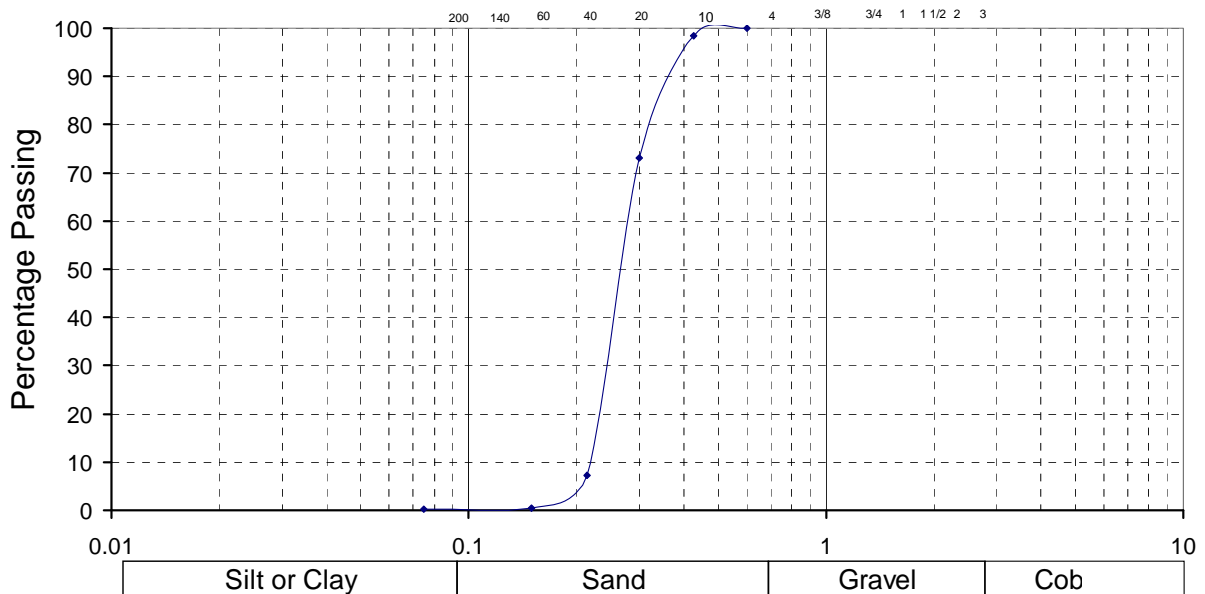


Figure 1. Particle size distribution curve of the soil.

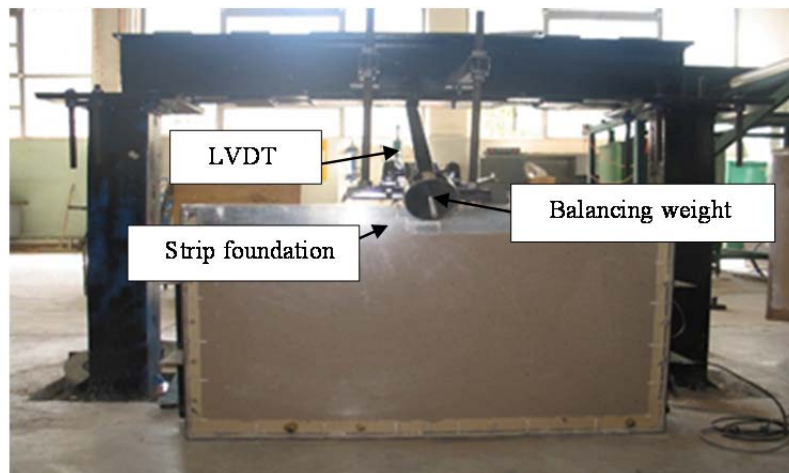


Figure 2. The laboratory test setup.

of plates with a width of 5.13 cm and a thickness of 3.34 mm were welded to the edges of the walls from outside to prevent lateral deformation under the lateral pressure of the soil. To observe the deformation of the soil mass and photograph the system during consecutive loading, one of the walls was made with a 30 mm thick transparent plexiglass of size 60×100 cm, which was connected by screws to three other plates. The load was centrally applied by a force-controlled system, in an incremental manner until failure. The applied load was measured by a digital load cell, which was connected directly to a data logger. To transfer the applied load to the soil, a rigid metal plate with a thickness of 0.36 cm and dimensions of 0.3×0.061 m was placed on the soil surface to act as the shallow strip foundation. The displacement of the plate was measured by a linear Variable Differential Transformer (LVDT),

which was installed on the plate close to its center. The displacements measured by LVDT were taken as settlement of the plate.

Figure 3a shows the number of reinforcement layers (N), the depth of the first reinforcement layer (u), the width of the reinforcements (b), and the width of the strip foundation (B). A schematic representation of the laboratory test setup is shown in Figure 3b.

One of the key requirements in setting up physical models is to make sure that the model is uniform. This requires maintaining consistency and continuity when placing the soil in the container. For this purpose, the soil should be poured linearly and uniformly into the test tank. In all models of this study, soil placement was performed using the pluviation method along both horizontal and

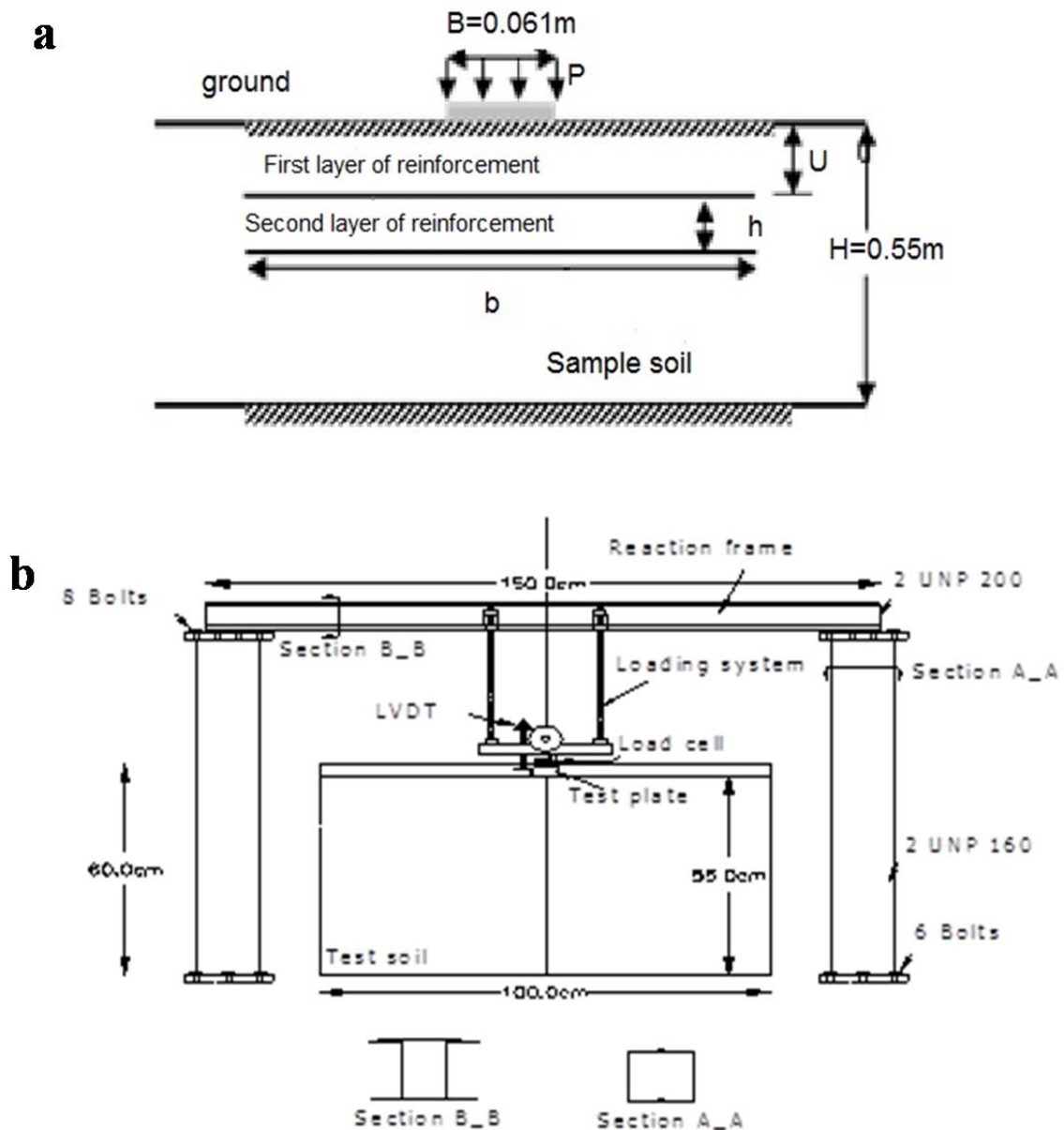


Figure 3. The laboratory test setup: a- Parameters of the model, b- The test setup.

vertical directions to achieve perfect uniformity. After pouring the soil to the height at which the reinforcement was to be placed, the surface was smoothen, and the reinforcement was placed in position before pouring continued to the next reinforcement level. This process continued until the required depth was attained. The strip foundation model was then gently placed on the surface of the soil below the lever of the loading system and the LVDT and force meter were installed. The loading was done manually. After each instance of loading, the load and settlement were recorded by the data logger and the system was photographed with a digital camera. The images were processed using Geopiv8 software (Adrian, 1991). Particle image velocimetry (PIV) is an optical method of flow visualization used in education and research. A modified approach to the application of PIV has been developed in

geotechnical experiments in which soil deformation is expressed as a low-velocity flow (White et al., 2003). While the fluid needs to be partitioned with particles (polystyrene balls or colored powder) to provide recognizable texture and image characteristics so that image processing can be applied, sand naturally has the inherent texture of different colored particles. During PIV, the particle concentration is such that it is possible to identify individual particles in an image, but not with certainty to track it between images. When the particle concentration is so low that it is possible to follow an individual particle it is called particle tracking velocimetry, while Laser speckle velocimetry is used for cases where the particle concentration is so high that it is difficult to observe individual particles in an image. Typical PIV apparatus consists of a camera (normally a digital camera with a CCD chip in

Table 1. Specifications of models made in the laboratory and Plaxis.

The number of test	1	2	4	5	6	7	8
Reinforced type	A	A	A	A	A	B	Non-reinforced
N	1	1	1	1	1	1	-
b/B	15	15	15	11	9	15	-
u/B	5/0	25/0	1	5/0	5/0	5/0	-
h/B	5/0	-	-	-	-	-	-

In this table, N is number of reinforcement, b the reinforcement width, u the distance of the first reinforcement layer, h the distance between the reinforcements and B the width of the foundation.

Table 2. Specifications of sandy soil, reinforcements, and foundation in the laboratory model and numerical simulation.

Angle of internal friction of the sandy soil (ϕ)	26.82
Specific gravity of sand (KN/m^3)	15
Soil-reinforcement friction angle (Rinter)	0.9
Grain density (Gs)	2.67
Weight of reinforcement (g/m^3)	300
Thickness of reinforcement (mm)	1.6
Maximum tensile strength of geotextile and geogrid (KN/m)	13, 55
Elastic modulus of sandy soil - E (KN/m^3)	8000
Axial stiffness of geotextile and geogrid - EA (KN/m)	1000, 1500

modern systems), a strobe or laser with an optical arrangement to limit the physical region illuminated (normally a cylindrical lens to convert a light beam to a line), a synchronizer to act as an external trigger for control of the camera and laser, the seeding particles.

The photographs taken were partitioned into 48x48 meshes to obtain a suitable image texture for analysis of the displacement of the meshes in the changing soil mass. The deformations and failure mechanism of the soil were then investigated. For the parametric study of the effect of reinforcements, the tests were performed with geogrids or geotextiles, placed in different numbers and at different spacings. The effect of arrangement of the geotextiles was also examined. The parameters of the laboratory and numerical models are listed on Table 1. The specifications of the materials used in the models are provided on Table 2 (in this table, geotextiles are marked with A and geogrids with B).

Numerical simulation

The numerical analysis was performed using finite element method with PLAXIS v8.2 software. The soil model was developed using the Mohr-Coulomb model in the plane strain state and by the use of 15-node elements to ensure sufficient accuracy. The reinforcement was modeled with geogrid elements, which cannot withstand bending. The upper and lower surfaces of the reinforcement were given the same amount of roughness. To make the results comparable, the numerical and laboratory models were given the same specifications. It was assumed that there is no friction between the soil and the walls of the container and that the walls are rigid. Accordingly, the base of the geometry was assigned with completely fixed boundary conditions and the vertical sides were given roller boundary conditions. Assuming that the foundation is

rigid, the settlement of the foundation was simulated by a uniform indentation on top of the sand layer instead of modeling the foundation itself to simplify the calculations. Considering the relocation of the reinforcements with the change in meshing, attempt was made to minimize effect of meshing in the model and therefore, the prescribed displacement option was used to apply the settlement to the strip foundation.

RESULTS AND DISCUSSION

Effect of reinforcement type on the load-bearing capacity of the strip foundation in physical and numerical models

Figure 4a shows the load-settlement plot of the strip foundation model is on the non-reinforced soil, and the soil reinforced with geotextiles and geogrids. This study used two types of reinforcement: geogrid and geotextile. For geotextile, the direct sliding resistance between the soil and the geotextile takes place on their interface, but for geogrid, it is associated with sliding of soil on the soil grains in the geogrid holes and on the geogrid itself. Therefore, the shear strength produced by geogrid is much higher than that of geotextile. Figure 4 shows the load-settlement for the two types of reinforcement (at a depth of $u=30$ mm) and also for the non-reinforced state.

In Figure 4a, for loads below 50 kPa, the curve of the geogrid-reinforced model is below that of the geotextile

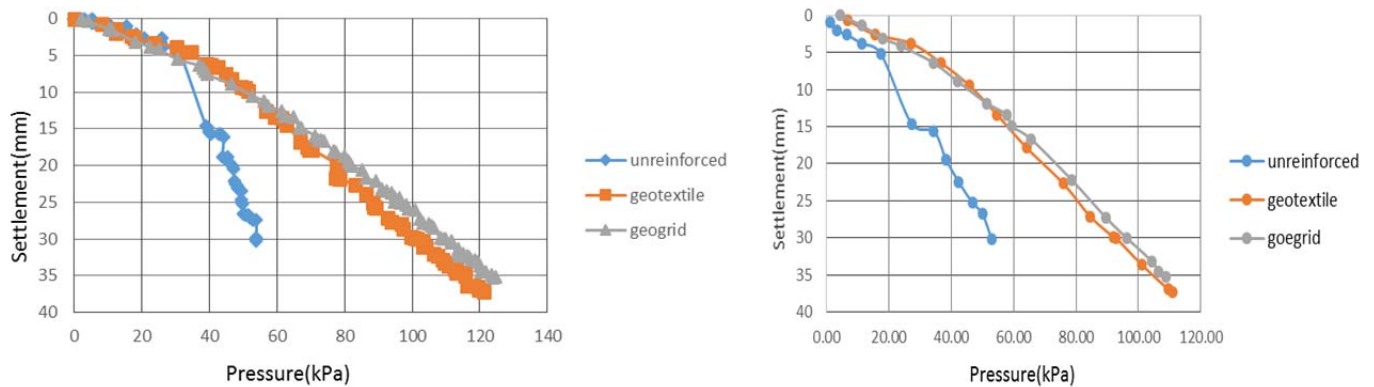


Figure 4. Load-settlement plots: a-laboratory models, and b - numerical models.

reinforced model, but the opposite is true for loads above 50 kPa. According to Guido et al. (1986) at lower loads, reinforcements with low tensile strength perform better than those with high tensile strength. This plot also demonstrates the superiority of both geogrid and geotextile reinforced models over the non-reinforced models. The non-reinforced foundation fails at the load of 36 kPa, after which a small increase in the load results in a large settlement. The geogrid and geotextile reinforced foundations, however, do not undergo sudden failure until loads of 124 and 121 kPa respectively.

In the plot of the non-reinforced model, the settlement increases with increasing load, but the failure surface in the soil gradually expands outward, and there is a sudden jump in the settlement of the foundation when the load reaches 36 kPa. Beyond this point, a significant settlement is needed for the failure surface to reach the ground surface. At this point, the load-settlement curve has a relatively sharp slope, which signifies local shear failure mechanism. In the geogrid-reinforced, geotextile-reinforced, and non-reinforced models, the load at which the foundation settlement reaches 30 mm is 110, 101 and 54 kPa, respectively. As shown in Figure 4b, the non-reinforced foundation base fails at 18 kPa, after which a small increase in the load causes significant settlement. The reinforced foundation bases, however, do not exhibit sudden failure. In the geogrid-reinforced, geotextile-reinforced, and non-reinforced models, the load at which the foundation settlement reaches 30 mm is 96, 92 and 53 kPa, respectively. Therefore, both physical and numerical models predict better performance in the reinforced state than the non-reinforced base and that geogrid performs better than geotextile.

Effect of number of reinforcement layers on the load-bearing capacity of the strip foundation in physical and numerical models

The effect of the number of reinforcement layers is shown

in Figure 5. Figure 5a compares results of the models in which one or two layers of geotextile were used and the corresponding non-reinforced model. It should be noted that the spacing between the geotextile layers is 30 mm. As shown in the figure, at each given load, the model with two layers of geotextiles has fewer settlements than that with one layer of geotextile. It is evident that as the number of layers increases, the reinforced soil foundation becomes more compact, which means that a large mass of the soil must move for settlement to occur. Therefore, the resistance against soil displacement increases, translating to less settlement. Figure 5b shows results of the numerical model. This figure also shows that, at each given load, the presence of two layers of geotextile results in less settlement than one layer.

Effect of the depth of first reinforcement layer (u) on load-bearing capacity of the strip foundation in physical and numerical models

Figure 6 show the changes in the load-settlement relationship with changes in u/B ratio in the physical and numerical models. As shown in Figure 6a, under loads below 70 kPa, the model with $u/B=1$ performed better than the other two models. But under larger loads (>70 kPa), the model with $u/B=0.5$ experienced less settlement than the other two models. This result is consistent with the findings of Gabr et al. (2000) who reported a critical depth of $u/B=0.5$ for sandy soil. Demerchant et al., (2002) reported a critical depth of $u/B=0.25$ for light aggregates. According to Figure 6, the critical depth is between $u/B=0.5$ and $u/B=1.0$ for small loads and between $u/B=0.25$ and $u/B=0.5$ for large loads.

Figure 6b shows the results obtained from the numerical model. As can be seen, under large loads, the model with $u/B=1.0$ performed better than the other two models. Under small loads, however, the model with $u/B=0.50$ has smaller settlements than the other two

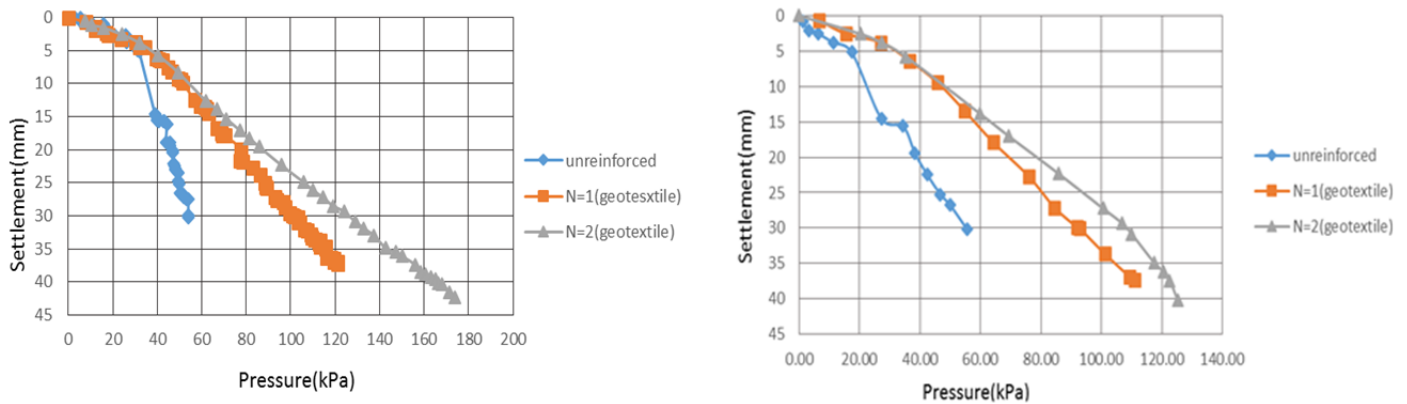


Figure 5. Load-settlement plots: a - laboratory models, b - numerical models.

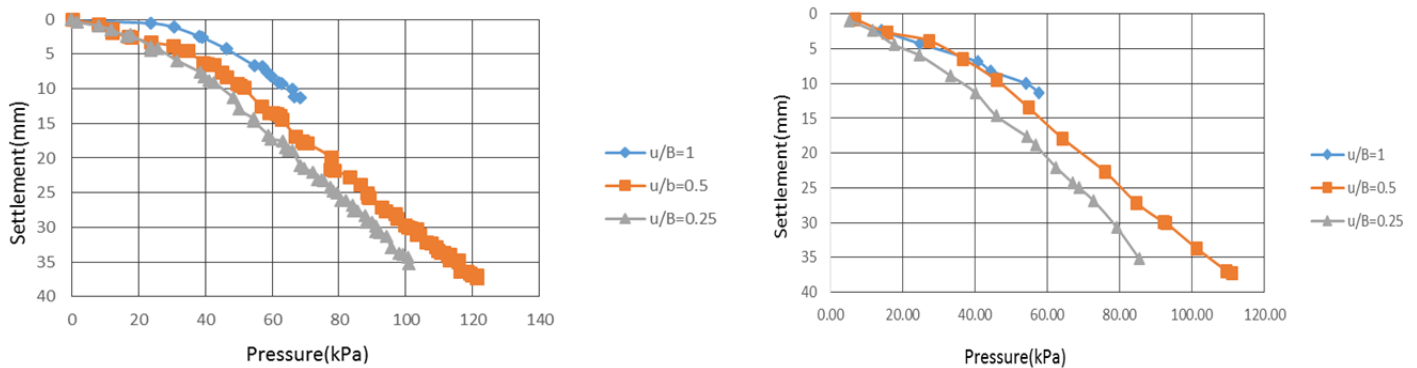


Figure 6. Load-settlement plots: a - laboratory models with different u/B ratios; b - numerical models with different u/B ratios.

models. Generally, these results show the existence of a critical depth at $u/B=0.65$ for sandy soil.

Effect of the width of reinforcement (b) on load-bearing capacity of the strip foundation in physical and numerical models

Figure 7 shows the load-settlement plots obtained for the models with one layer of geotextile reinforcement and b/B ratios of 9 and 11, positioned at a depth of $u=30$ mm. As shown in Figure 7a, at low settlements, there is no significant increase in load-bearing capacity with increase in b/B ratio, but the models with higher b/B ratio undergo smaller settlements under the same loads. This is attributed to increased contact of the sand with the reinforcement, which resulted in larger frictional force and consequently higher shear strength.

Figure 7b shows effect of width of the reinforcement in the numerical models. As this figure shows, the presence of wider reinforcements led to greater increase in the load-bearing capacity of the soil.

Effect of type and number of reinforcements on the ultimate bearing capacity ratio (UBCR) of the strip foundation in physical and numerical models

Ultimate bearing capacity ratio (UBCR) was used to compare load-bearing capacity of the reinforced and non-reinforced models with each other. This ratio was defined as $UBCR=qr/qu$, where qr is the ultimate bearing capacity of the strip foundation in the reinforced state and qu is the ultimate bearing capacity of the same strip foundation in the non-reinforced state for a fixed settlement of 30 mm.

As shown in Figure 8a, for geogrid and geotextile reinforcements with $u/B=0.5$, UBCR was calculated to be 2 and 1.85 respectively (changing the reinforcement resulted in a 2-fold increase in UBCR for geogrid and a 1.85-fold increase in UBCR for geotextile).

Figure 8b shows the effect of the number of geotextile reinforcement layers at $u/B=0.5$. As the figure shows, increasing the number of geotextile layers from one to two increased UBCR from 1.85 to 2.31.

As shown in Figure 9a, the numerical model predicted that UBCR for geogrid and geotextile reinforcements with

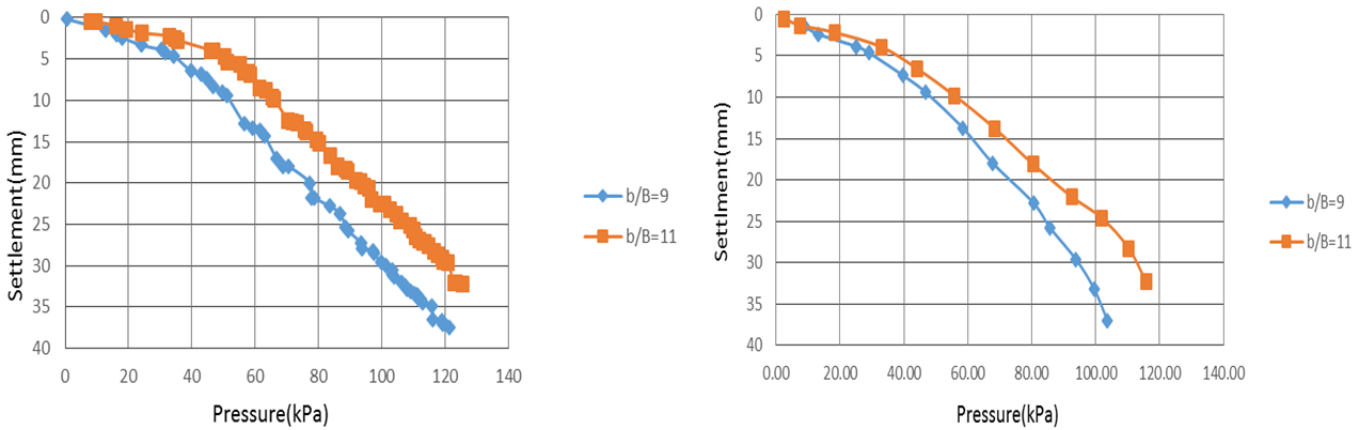


Figure 7. Load-settlement plots: a - laboratory models; b - numerical models.

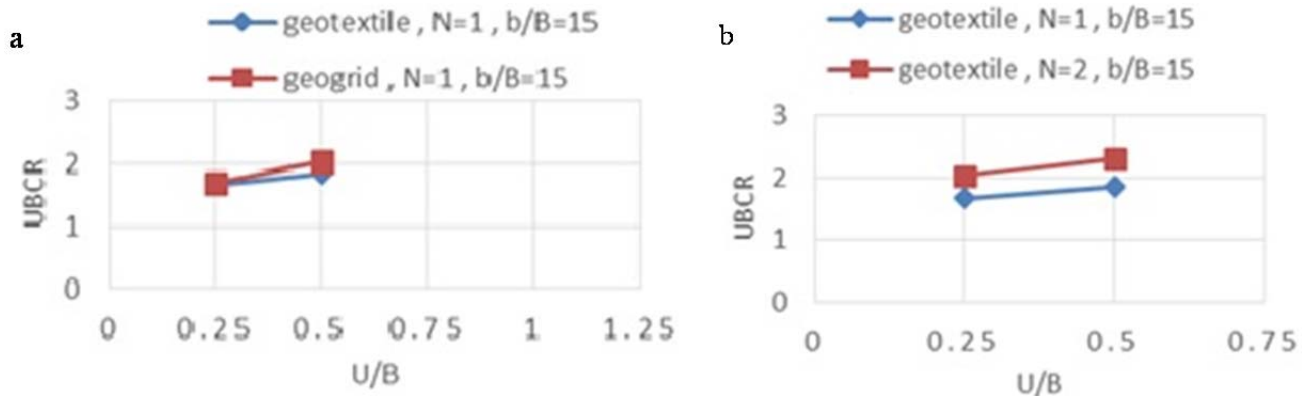


Figure 8. a and b - the ultimate bearing capacity ratio (UBCR) of the laboratory models.

$u/B=0.5$ would be 1.81 and 1.73 respectively. Figure 9b illustrates effect of the number of geotextile reinforcement layers at $u/B=0.5$ from the numerical model. As can be seen, the model predicted that increasing the number of geotextile layers from one to two would increase UBCR from 1.73 to 2.07.

Mechanism of the soil behavior

Throughout the test, the soil mass was photographed by a digital camera to monitor its deformations following the occurrence of certain displacements in the strip foundation. The obtained images were processed using PIV software. Figure 10 shows the displacement vectors, obtained from image processing at the stage where the non-reinforced and geotextile-reinforced (single layer) soil, with $S/B=0.5$ (where S denotes settlement and is 30 mm) have a completely formed failure wedge. By comparing these two images, it can be seen that the

failure wedge of the reinforced model has expanded more in depth and width than that of the non-reinforced model. Figure 10a shows that the slicing starts right below the foundation, from its outer edge. In Figure 10b, it can be seen that the failure wedge begins to form immediately below the geotextile layer. The displacement vectors above the reinforcement layer are not aligned with those below the layer. Above the geotextile layer, a series of local failure surfaces have been formed (marked with red arrows). Figures 10 c and d show the displacement vectors, obtained from the Plaxis analysis of non-reinforced and geotextile-reinforced (single layer) models with $S/B=0.5$. In Figure 10c, as the depth increased, the vectors become smaller and more downward. In Figure 10d, the displacement vectors below the reinforcement layer are downward. The vectors in this section are larger, which results in deformation of the reinforcement layer below the foundation. The failure wedge has started to form immediately below the geotextile layer. In the reinforced models, the failure

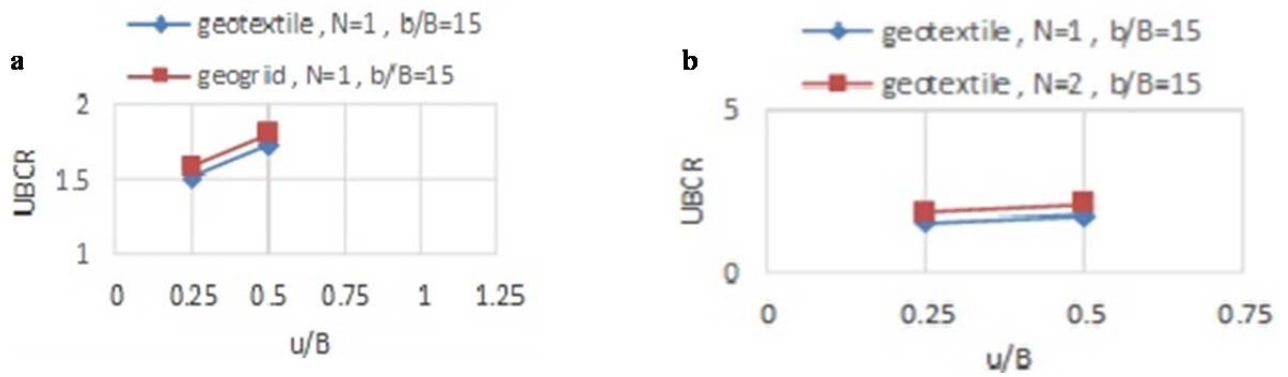


Figure 9. a, b- the ultimate bearing capacity ratio (UBCR) of the numerical models.

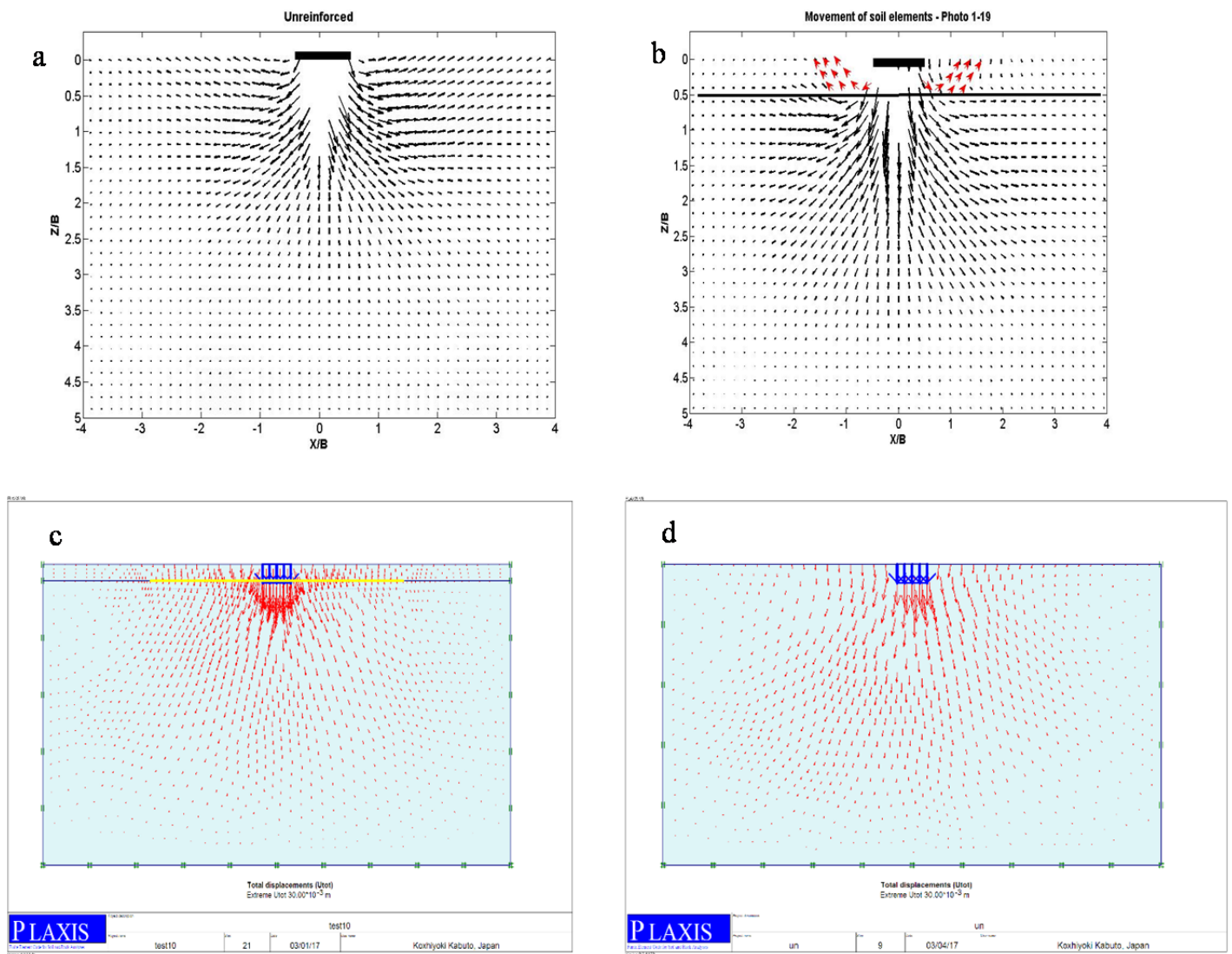


Figure 10. Failure surfaces in the laboratory and numerical models of non-reinforced soil and soil with one layer of reinforcement with the settlement of $S/B = 0.5$. a, b: Unreinforced soil and reinforced soil in laboratory models. c, d: Unreinforced soil and reinforced soil in numerical models.

Table 3. The relative error rate of the tests.

Excremental number	1	2	3	4	5	6	7	8
Relative error values	9	15	16	15	11	11	15	12

surfaces have reached below the reinforcement layer but not the ground surface. These models also show deeper and wider failures, compared to non-reinforced states. In these models, the reinforced section acts as a composite gravity structure, which transfers the foundation loads to the lower layers outside the failure wedge, thereby increasing the bearing capacity of the foundation.

To compare the performance of physical and numerical models, the relative error for the load parameter in all tests was calculated. A smaller relative error indicates a better and more complete model. The relative error was computed by the following formula:

$$\text{relative error} = \left| \frac{y_i - y_j}{y_i} \right|$$

The relative error values obtained for the tests are listed in Table 3.

The above values indicate the proximity of the absolute error (the difference between laboratory and numerical results) to the actual value (laboratory results).

Conclusion

In this study, a series of laboratory and numerical models were used to compare the load-bearing capacity of strip foundations, resting on loose sandy soil. Considering the limitations of the study in terms of the impact of size and other parameters of the laboratory model on the results, the following conclusions are made: The numerical and laboratory models of this study showed that the use of reinforcement in non-reinforced soils can greatly increase the load-bearing capacity of strip foundations. The reinforced soils have a larger failure surface with a deeper wedge than the non-reinforced soils (Terzaghi's bearing capacity theory).

The best type of reinforcement to achieve good performance and ultimate bearing capacity ratio was found to be geogrid, which resulted in a 2 times increase in the bearing capacity of the laboratory model and 1.81 times increase in the numerical model (compared to non-reinforced state)

Increasing the number of reinforcement layers also increased the bearing capacity. The use of two reinforcement layers instead of one increased the ultimate bearing capacity ratio of the laboratory model and the numerical model to 2.31 and 2.07, respectively.

There was a good agreement between numerical and laboratory results. However, the numerical model slightly underestimated the experimental results. This can be attributed to slight inconsistencies between the behaviors of sandy soil and reinforcements in the numerical models and those in the laboratory models, the conditions considered for the plane strain state in the model, the negative impact of wall friction in the laboratory model (which we attempted to minimize), the interaction between the foundation, the soil, and reinforcements, and the type of numerical model (Mohr-Coulomb).

Since the laboratory tests were conducted on a scaled-down model and the materials do not behave perfectly similar to how they behave in reality, to achieve more accurate results, the test should be repeated with models of larger scales. Also, this study only examined the behavior of the soil and reinforcement and did not consider stiffness of the reinforcements.

CONFLICT OF INTERESTS

The authors have not declared any conflict of interests.

REFERENCES

- Adrian RJ (1991). "Particle-imaging techniques for experimental fluid mechanics." Annual review of fluid mechanics 23(1):261-304. <https://doi.org/10.1146/annurev.fl.23.010191.001401>
- Alaminiokuma GI, Omigie JI (2020). Anisotropic properties of the near-surface in South-Western Niger Delta: Implications on geotechnical constructions. Journal of Geology and Mining Research 12(1):1-12. <https://doi.org/10.5897/JGMR2019.0314>
- Bergado DT, Long PV, Murthy BS (2002). A case study of geotextile-reinforced embankment on soft ground. Geotextiles and Geomembranes 20(6):343-365. [https://doi.org/10.1016/S0266-1144\(02\)00032-8](https://doi.org/10.1016/S0266-1144(02)00032-8)
- Biquet J, Lee KL (1975). Bearing capacity tests on reinforced earth slabs. Journal of Geotechnical and Geoenvironmental Engineering 101(ASCE# 11792 Proceeding).
- Chen Q, Abu-Farsakh M (2015). Ultimate bearing capacity analysis of strip footings on reinforced soil foundation. Soils and Foundations 55(1):74-85. <https://doi.org/10.1016/j.sandf.2014.12.006>
- Daoud AM, Rashed MA, Elsharief AM, Sediek KN, Elamein AM (2020). The geotechnical properties of the oolitic ironstone formation, Wadi Halfa, North Sudan. Journal of Geology and Mining Research 12(1):25-34. <https://doi.org/10.5897/JGMR2019.0326>
- Das BM (2017). Shallow foundations: bearing capacity and settlement. CRC Press.
- DeMerchant MR, Valsangkar AJ, Schriver AB (2002). Plate load tests on geogrid-reinforced expanded shale lightweight aggregate. Geotextiles and Geomembranes 20(3):173-190. [https://doi.org/10.1016/S0266-1144\(02\)00006-7](https://doi.org/10.1016/S0266-1144(02)00006-7)
- Gabr MA, John H, Hart S (2000). "Elastic modulus of geogrid-reinforced

- sand using plate load tests." *Geotechnical Testing Journal* 23(2):245-250. <https://doi.org/10.1520/GTJ11049J>
- Guido Vito A, Dong K, Chang, Michael A (1986). Sweeney. "Comparison of geogrid and geotextile reinforced earth slabs." *Canadian Geotechnical Journal* 23(4):435-440. <https://doi.org/10.1139/t86-073>
- Huang CC, Menq, FY (1997). Deep-footing and wide-slab effects in reinforced sandy ground. *Journal of Geotechnical and Geoenvironmental Engineering* 123(1):30-36. [https://doi.org/10.1061/\(ASCE\)1090-0241\(1997\)123:1\(30\)](https://doi.org/10.1061/(ASCE)1090-0241(1997)123:1(30)).
- Kothari UC, Momayez M (2018). "New approaches to monitoring, analyzing and predicting slope instabilities." *Journal of Geology and Mining Research* 10(1):1-14. <https://doi.org/10.5897/JGMR2017.0272>
- Oyawale AA, Ocan OO (2020). Migmatization process and the nature of transition from amphibolite to granulite facies metamorphism in Ikare area south western Nigeria. *Journal of Geology and Mining Research* 12(2):45-64. <https://doi.org/10.5897/JGMR2020.0334>
- Satvati S, Alimohammadi H, Rowshanzamir MA, Hejazi SM (2020). "Bearing Capacity of Shallow Footings Reinforced with Braid and Geogrid Adjacent to Soil Slope", *International Journal of Geosynthetics and Ground Engineering* 6(4):1-12.
- Satvati S, Rowshanzamir MA, Hejazi SM (2016a) "Evaluation of the Bearing Capacity of Shallow Footing on Soil Slope Reinforced by Braid Elements", 3rd American Conference on Geosynthetics, GeoAmericas 2016, Miami, USA.
- Satvati S, Rowshanzamir MA, Hejazi SM (2016b). "A Comparison Between the Bearing Capacities of Strip Footing on Soil Slope Reinforced by 2 Dimensional and 3 Dimensional New Braid Elements and Geogrid Elements", 3rd American Conference on Geosynthetics, GeoAmericas 2016, Miami, USA.
- Wu Y, Ashlock J, Cetin B, Satvati S, Li C, Ceylan H (2020). "Mechanistic Performance Evaluation of Chemically and Mechanically Stabilized Granular Roadways", ASCE Geo-Congress 2020: Vision, Insight, Outlook, Minneapolis, MN. <https://doi.org/10.1061/9780784482810.061>
- Yamamoto K (1998). "Failure mechanism of reinforced foundation ground and its bearing capacity analysis." Doctoral Thesis, Kumamoto University. <https://doi.org/10.11501/3145583>.